INTERNATIONAL JOURNAL FOR NUMERICAL METHODS IN FLUIDS, VOL. 5, 257–268 (1985)

APPLICATION OF THE TWO-EQUATION k–ε TURBULENCE MODEL TO A TWO-DIMENSIONAL, STEADY, FREE SURFACE FLOW PROBLEM WITH SEPARATION

RAYMOND S. CHAPMAN*

Offshore and Coastal Technologies, Inc., Vicksburg, Mississippi 39180, U.S.A.

AND

CHIN Y. KUO†

Department of Civil Engineering, Virginia Polytechnic Institute and State University, Blacksburg, Virginia 24061, U.S.A.

SUMMARY

An application of the depth-integrated k–ε turbulence model is presented for separated flow in a wide, shallow, rectangular channel with an abrupt expansion in width. The well-known numerical problems associated with the use of upwind and central finite differences for convection are overcome by the adoption of the spatially third-order accurate QUICK finite difference technique. Results show that modification of the depth-integrated k–ε turbulence closure model for streamline curvature leads to significant improvement in the agreement between model predictions and experimental measurements.

KEY WORDS Turbulence Model Finite Difference QUICK Free Surface Flow Channel Expansion

INTRODUCTION

Many of the free surface flow problems encountered by hydraulic engineers can be suitably analysed by means of the depth-integrated equations of motion. A consequence of adopting a depth-integrated modelling approach is that closure approximations must be implemented to represent the so called effective stresses.[1]

The effective stresses, as defined by Kuipers and Vreugdenhil,[2] consist of the depth-integrated viscous stresses, which are usually negligible, the depth-integrated turbulent Reynolds stresses, and additional stresses resulting from the depth-integration of the non-linear convective accelerations (here after called momentum dispersion). Existing closure schemes for momentum dispersion[1,3] lack sufficient numerical and experimental verification to warrant consideration at this time, so attention is consequently focused on examining closure for the depth-integrated turbulent Reynolds stress.

In this paper, a test application of the depth-integrated k–ε turbulence closure model is presented for separated flow in a wide, shallow, rectangular channel with an abrupt, symmetric expansion in width (Figure 1). The numerical technique employed is the spatially third-order

*Vice President
†Professor; addressee for correspondence

0271–2091/85/03 0257–12$01.20

Received 30 January 1984
Revised 9 March 1984

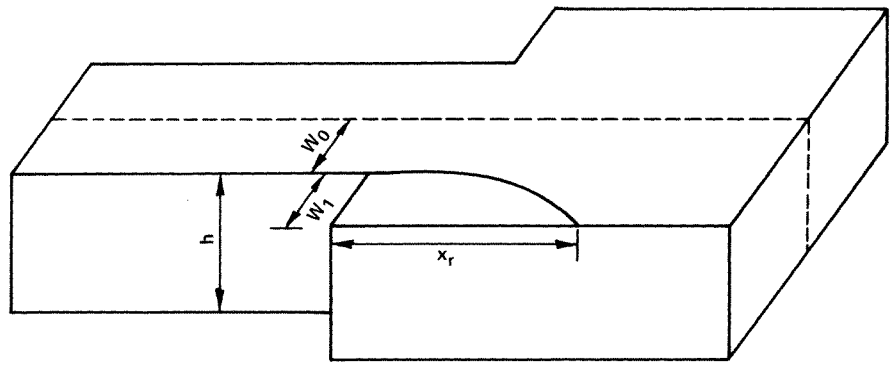

Figure 1. Definition sketch for a channel expansion

accurate QUICK (quadratic upstream interpolation for convective kinematics) finite difference method of Leonard.[4] The performance of the depth-integrated k–ε turbulence closure model is evaluated by comparison of numerical results with experimental measurements of flow past a rearward-facing step.[5]

DEPTH-INTEGRATED EQUATIONS OF MOTION

Under the assumption of a homogeneous, incompressible, viscous flow characterized by a hydrostatic pressure distribution, with wind and Coriolis forces neglected, the depth-integrated equations of motion are written[2]

$$\frac{\partial h}{\partial t} + \frac{\partial (V_m h)}{\partial X_m} = 0 \tag{1}$$

$$\frac{\partial (V_m h)}{\partial t} + \frac{\partial (V_m V_n h)}{\partial X_n} + g\frac{\partial (h^2/2)}{\partial X_m} + gh\frac{\partial z_b}{\partial X_m} + \tau_{bm} - \frac{\partial T_{mn}}{\partial X_n} = 0 \tag{2}$$

in which m, $n = 1$, 2 and repeated indices require summation, V_m = two-dimensional depth-averaged velocity vectors (U, V), h = water depth, t = time, X_m = co-ordinate directions (x, y), g = acceleration due to gravity, z_b = channel bottom elevation above an arbitrary datum, τ_{bm} = components of the bottom shear stress per unit mass and T_{mn} = components of the depth-integrated effective stress tensor per unit mass.[6] The bottom stress terms are parameterized in accordance with the quadratic shear stress law, namely

$$\tau_{bm} = cV_m q \tag{3}$$

where $q = (U^2 + V^2)^{1/2}$ is the magnitude of the depth-averaged resultant velocity vector and c is a friction coefficient. The depth-integrated effective stress tensor per unit mass is written

$$T_{mn} = \int_{z_b}^{h+z_b} \left[\nu \left(\frac{\partial v_m}{\partial X_n} + \frac{\partial v_n}{\partial X_m} \right) - \overline{v'_m v'_n} - (v_m - V_m)(v_n - V_n) \right] dz \tag{4}$$

in which ν = kinematic viscosity, v'_m = horizontal turbulent velocity fluctuations, v_m = three dimensional time averaged velocity components and z = vertical co-ordinate direction. The contributions to the effective stress tensor (equation (4)) are the viscous stresses, Reynolds stresses and momentum dispersion, respectively. In the present work, momentum dispersion is neglected, and attention is focused on closure of the depth-integrated Reynolds stresses.

TURBULENCE CLOSURE MODEL

The turbulence closure model adopted to represent the depth-integrated Reynolds stresses is a modification of the depth-integrated k–ε turbulence model presented by Rastogi and Rodi.[7] The depth-integrated k–ε turbulence model, which is based on a Boussinesq eddy viscosity hypothesis,[8] relates the depth-integrated Reynolds stresses to the depth-integrated strain rates by

$$-\int_{z_b}^{h+z_b} v'_m v'_n \, dz = \hat{\nu}_t \left[\frac{\partial(V_m h)}{\partial X_n} + \frac{\partial(V_n h)}{\partial X_m} \right] - \tfrac{2}{3} \hat{k} h \delta_{mn} \tag{5}$$

where the caret denotes depth-averaged values. The depth-averaged kinematic eddy viscosity, $\hat{\nu}_t$, is computed from

$$\hat{\nu}_t = C_\mu \frac{\hat{k}^2}{\hat{\varepsilon}} \tag{6}$$

where the distribution of the depth-averaged turbulence kinetic energy per unit mass, $\hat{k}$, and its rate of dissipation, $\hat{\varepsilon}$, are determined by the solution of the following transport equations, which when written in conservation form read:

$$\frac{\partial(\hat{k}h)}{\partial t} + \frac{\partial(V_m \hat{k} h)}{\partial X_m} = \frac{\partial}{\partial X_m} \left[\frac{\hat{\nu}_t}{\sigma_k} \frac{\partial(\hat{k}h)}{\partial X_m} \right] + P_h + P_k - \hat{\varepsilon} h \tag{7}$$

$$\frac{\partial(\hat{\varepsilon}h)}{\partial t} + \frac{\partial(V_m \hat{\varepsilon} h)}{\partial X_m} = \frac{\partial}{\partial X_m} \left[\frac{\hat{\nu}_t}{\sigma_\varepsilon} \frac{\partial(\hat{\varepsilon}h)}{\partial X_m} \right] + \frac{\hat{\varepsilon}}{\hat{k}} (C_1 P_h - C_2 \hat{\varepsilon} h) + P_\varepsilon \tag{8}$$

in which

$$P_h = \frac{\hat{\nu}_t}{h} \left[\frac{\partial(V_m h)}{\partial X_n} + \frac{\partial(V_n h)}{\partial X_m} \right] \frac{\partial(V_m h)}{\partial X_n} \tag{9}$$

The source terms P_k and P_ε are included in the depth-integrated version of the k–ε model to account for the production mechanism due to the vertical boundary layer. Following Rastogi and Rodi,[7] the source terms written in a conservation form consistent with equations (7)–(9) read

$$P_k = cq^3 \tag{10}$$

and

$$P_\varepsilon = \frac{C_2 C_\mu c^{5/4} q^4}{h D^{1/2}} \tag{11}$$

where c and D are the non-dimensional friction and dispersion coefficients, respectively, which are defined under conditions of uniform flow along the centerline of an open channel. Experience indicates[9] that for smooth channels an assumption of D equal to 1·0 and $c = 0{\cdot}0045$ is quite satisfactory.

The values of the empirical constants found in equations (6)–(8), $C_1 = 1{\cdot}44$, $C_2 = 1{\cdot}92$, $C_\mu = 0{\cdot}09$, $\sigma_k = 1{\cdot}0$ and $\sigma_\varepsilon = 1{\cdot}3$, are those recommended by Launder and Spalding.[10]

COMPUTATIONAL METHOD

The numerical technique employed to obtain approximate solutions for the depth-integrated model equations is the third-order interpolation technique, QUICK. The QUICK finite difference technique, which is based on a conservative, control-volume integral formulation, possesses the desirable convective stability of upwind differencing, but is free of classical numerical diffusion.

To apply QUICK in a depth-integrated transport model, each equation is integrated over its

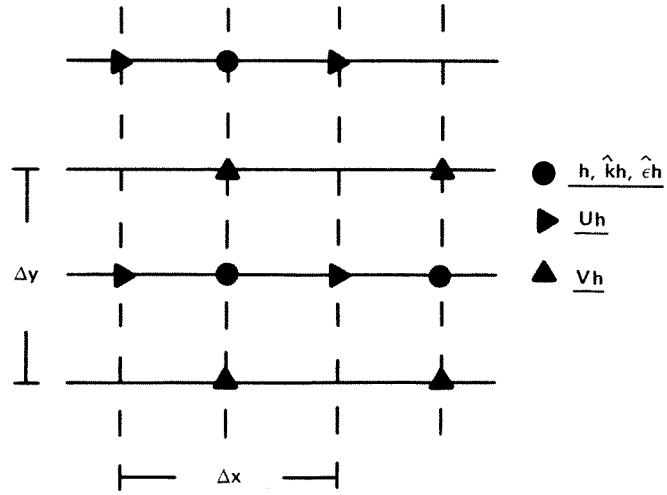

Figure 2. Computational grid

appropriate control cell on a constant space, staggered, square computation grid (Figure 2) and in time. For purposes of generality, the model equations can be written in the following vector form:

$$\frac{\partial Ft}{\partial t}+\frac{\partial Fx}{\partial x}+\frac{\partial Fy}{\partial y}=G \tag{12}$$

where

$$Ft=\begin{bmatrix} h \\ Uh \\ Vh \\ \hat{k}h \\ \hat{\varepsilon}h \end{bmatrix}; \qquad Fx=\begin{bmatrix} Uh \\ UUh+\dfrac{gh}{2}-T_{xx} \\ UVh-T_{xy} \\ U\hat{k}h-\hat{\nu}_t\dfrac{\partial}{\partial x}(\hat{k}h) \\ U\hat{\varepsilon}h-\dfrac{\hat{\nu}_t}{\sigma_\varepsilon}\dfrac{\partial}{\partial x}(\hat{\varepsilon}h) \end{bmatrix} \tag{13}$$

$$Fy=\begin{bmatrix} Vh \\ UVh-T_{xy} \\ VVh+\dfrac{gh}{2}-T_{yy} \\ V\hat{k}h-\hat{\nu}_t\dfrac{\partial}{\partial y}(\hat{k}h) \\ V\hat{\varepsilon}h-\dfrac{\hat{\nu}_t}{\sigma_\varepsilon}\dfrac{\partial}{\partial y}(\hat{\varepsilon}h) \end{bmatrix}; \qquad G=\begin{bmatrix} 0 \\ gh\dfrac{\partial z_b}{\partial x}+\tau_{bx} \\ gh\dfrac{\partial z_b}{\partial y}+\tau_{by} \\ P_h+P_k-\hat{\varepsilon}h \\ \dfrac{\hat{\varepsilon}}{\hat{k}}(C_1P_h-C_2\hat{\varepsilon}h)+P_\varepsilon \end{bmatrix}$$

in which all variables have been defined previously. Adopting a first-order, explicit time integration, the exact control cell integration of equation (12) is then written:

$$\mathbf{Ft}^{n+1}=\mathbf{Ft}^n-\frac{\Delta t}{\Delta s}[(Fx)_R-(Fx)_L+(Fy)_T-(Fy)_B]^n+\mathbf{G}^n\Delta t \tag{14}$$

in which quantities in parentheses with subscripts R, L, T and B denote right, left, top and bottom cell face averages, respectively, and bold-faced quantities denote cell averages. Although the ultimate interest of the present work is to achieve steady-state solutions, explicit time integration is retained as a suitable alternative to the use of iterative matrix reduction techniques which resort to linearization of the transport equations. It is well known that this is not the most efficient means of achieving a steady-state solution, however, it is a proven and well accepted technique.

The cell and cell face averages required in equation (14) are approximated by integrating a six-point upstream weighted quadratic interpolation function over appropriate limits. To illustrate this procedure, consider the computation of the right cell face average of a field variable, f, using the information provided in Figure 3. In this case, the U and V velocity components are both positive and directed to the right and up, respectively. Combining a Newton forward difference interpolation formula in the longitudinal, ξ, direction with a Gauss backward difference interpolation formula in the transverse, η, direction, a quadratic interpolation function is constructed which reads[11]

$$f_{\xi,\eta} = (1 - \xi^2 - \eta^2 - \xi\eta) f_{0,0} + \left(\frac{\xi^2}{2} + \frac{\xi}{2} + \xi\eta\right) f_{1,0} + \tfrac{1}{2}(\xi^2 - \xi) f_{-1,0} \tag{15}$$
$$+ \tfrac{1}{2}(\eta^2 + \eta) f_{0,1} + \left(\frac{\eta^2}{2} - \frac{\eta}{2} + \xi\eta\right) f_{0,-1} - \xi\eta f_{1,-1}$$

where $\xi = x/\Delta s$, and $\eta = y/\Delta s$ are local non-dimensional co-ordinates. The right cell face average is then computed as follows:

$$(f)_R = \int_{-1/2}^{1/2} f_{1/2,\eta}\, d\eta = \tfrac{1}{2}(f_{0,0} + f_{1,0}) - \tfrac{1}{8}(f_{1,0} - 2f_{0,0} + f_{-1,0}) + \tfrac{1}{24}(f_{0,1} - 2f_{0,0} + f_{0,-1}) \tag{16}$$

Owing to the symmetry of the integration operation, a change in the sign of the V velocity component will not alter equation (16). However, a change in the sign of the U velocity component will require that the mirror image of Figure 3 be used with the indices shifted to the right by one. Performing the integration prescribed in equation (16) results in the following interpolation

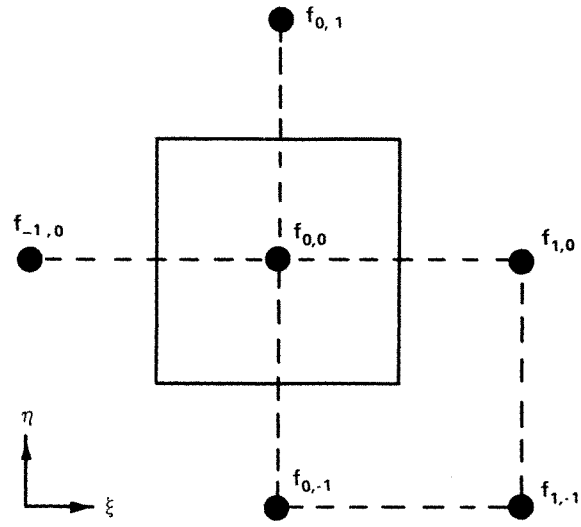

Figure 3. Nodal information required for a quadratic interpolation surface

formula:

$$(f)_R = \tfrac{1}{2}(f_{0,0} + f_{1,0}) - \tfrac{1}{8}(f_{2,0} - 2f_{1,0} - f_{0,0}) + \tfrac{1}{24}(f_{1,1} - 2f_{1,0} + f_{1,-1}) \tag{17}$$

The purpose of this adjustment is to maintain the upstream weighting of the interpolation formula.

MODEL SIMULATION

Model simulations were performed for flow in a wide, shallow, rectangular channel with an abrupt, symmetric expansion in width (Figure 1). The physical parameters specified were an aspect ratio ($= 1 + W_1/W_0$) of 1·45, a longitudinal channel slope of 0·0005, a transverse channel slope of zero and a friction coefficient of 0·0045, which corresponds to a channel roughness height, z_0, of 0·005 ft.

The normal velocity component and the normal gradient of the tangential velocity component, the normal gradient of the water surface elevation, and the normal gradient of the turbulence kinetic energy per unit mass were set to zero at rigid walls. Wall boundary values for the energy dissipation rate per unit mass and the shear stress were obtained by the 'wall function' method.[10] To apply the wall function method, it is necessary to assume that the near wall region is in local equilibrium so that the shear stress is constant and the logarithmic velocity law applies. Thus, the wall shear stress per unit mass is given by:

$$\tau_w = \frac{\kappa C_\mu^{1/4} \hat{k}_w^{1/2} U_w}{\ln\left(\dfrac{\Delta s}{2z_0}\right)} \tag{18}$$

where the value of the von Karman constant, κ, is defined to be 0·4 and the subscript w denotes values of the field variables located half a grid spacing from the wall. Similarly, within the constant shear stress layer, the turbulent length scale varies linearly; thus the near wall energy dissipation rate per unit mass is written

$$\hat{\varepsilon}_w = \frac{C_\mu^{3/4} \hat{k}_w^{3/2}}{\kappa\left(\dfrac{\Delta s}{2}\right)} \tag{19}$$

The near wall values of the velocity components, and the turbulence kinetic energy per unit mass were obtained from their respective balance equations with, however, the usual shear stress terms replaced by the wall shear stress (equation (18)). It should, however, be noted that defining boundary values for the shear stress and velocity gradient at the wall is in fact redundant. The requirement of a boundary condition for the velocity gradient at the wall is purely numerical, and unique to solution techniques that account for transverse curvature. Test simulations performed to investigate a variety of methods for extrapolating the velocity gradient at the wall revealed no significant difference in the form of the recirculation cell, so, consequently, as a matter of convenience the zero gradient condition was adopted.

A reflection boundary was enforced at the channel centreline by setting the normal velocity component, and the normal gradient of the remaining field variables to zero.

The water surface elevation at the upstream boundary was specified to have zero gradient in the transverse direction, zero curvature in the longitudinal direction, and a constant depth of 5·0 ft. This configuration corresponds to a unidirectional inflow boundary in which the transverse velocity component, V, was set to zero, and the longitudinal velocity component, U, was obtained from continuity. In addition, the turbulence quantities $\hat{k}h$ and $\hat{\varepsilon}h$ were assumed to have zero curvature in the longitudinal direction.

The downstream boundary configuration was essentially identical to the upstream boundary with the exception that the depth was initially set to 4·9 ft, for purposes of accelerating convergence, and then was allowed to vary as the solution evolved.

An initial condition for the k–ε turbulence closure simulations was generated by running a constant eddy viscosity version of the model to an approximate steady state. A steady state, constant eddy viscosity of 2·0 ft^2/s was found to be consistent with the earlier assumption on the value of the non-dimensional dispersion coefficient (i.e. $D = 1{\cdot}0$). An arbitrary initial condition was used in the constant eddy viscosity computation with the interior water surface elevations set to 5·0 ft, and the velocity components set to zero.

The computational region consisted of a 27 × 11 mesh upstream of the abrupt expansion, and a 77 × 16 mesh downstream of the expansion.

RESULTS AND DISCUSSION

In order to generate a region of recirculation, it was necessary to adopt a grid spacing of 5·0 ft, which ensured that the convective acceleration and the turbulent transport terms were the same order of magnitude as the bottom friction terms. Using a stable time step of 0·01 s and 4000 iterations, approximately 140 min of CPU time on an IBM 3032 was required to achieve a steady solution.

Results are presented in Figure 4, a vector plot of the depth-averaged resultant velocities, and Figures 5–7, comparisons of the predicted depth-averaged longitudinal velocity profiles with the experimental measurements of Moss *et al.*[5]

Experimental measurements of the non-dimensional reattachment length (x_r/W_1) have been found to vary significantly from one study to the next.[6,12] Consequently, for purposes of comparison, a number of experimental results are presented in Figure 8, a plot of published non-dimensional reattachment lengths as a function of the inlet channel aspect ratio (h/W_0). In the present work, the inlet channel aspect ratio was approximately 0·1, which suggests that the non-dimensional reattachment length should be about 4·5 to 5·0. However, it is seen in Figure 4 that the predicted non-dimensional reattachment length is only about 3·2.

The overall poor agreement between model predictions and experimental measurements is directly attributable to the over-prediction of the depth-averaged eddy viscosity in the region of strong streamline curvature. In an attempt to improve the model predictions, an approximation to the streamline curvature modification of Leschziner and Rodi[13] was employed. Leschziner and Rodi used a simplified algebraic Reynolds stress model to derive a streamline curvature dependent

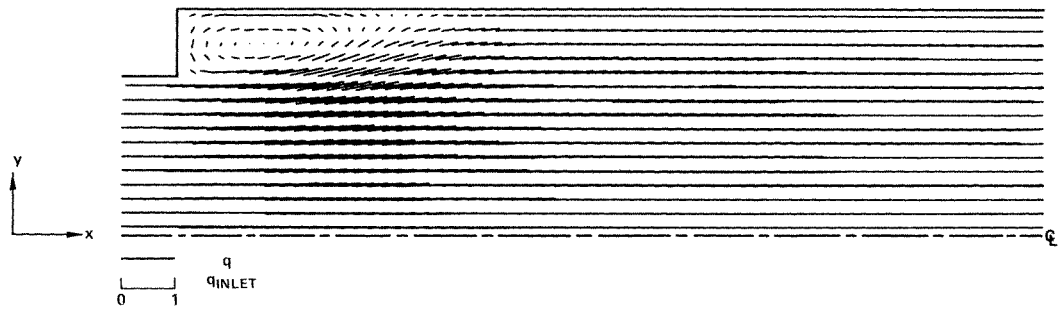

Figure 4. Depth-averaged velocity field for the standard (k–ε) model simulation. Note: grid points are located at the midpoints of the velocity vectors

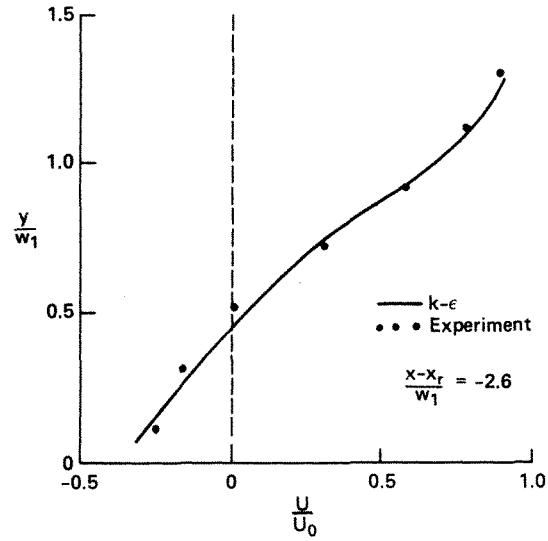

Figure 5. Comparison of standard (k–ε) model predictions with the experimental velocity measurements of Moss *et al.*[5]

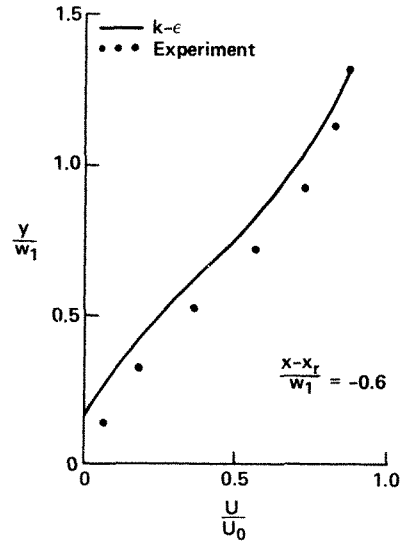

Figure 6. Comparison of standard (k–ε) model predictions with the experimental velocity measurements of Moss *et al.*[5]

form of the coefficient C_μ. The improved agreement between model predictions and experimental measurements of separated flow in annular and twin parallel jets, gained through use of the curvature modifications, suggested the validity of the argument that the value of C_μ is significantly reduced in regions of strong streamline curvature. Consequently, as a first approximation, the value of C_μ was decreased to 0·03 at all grid points interior to the wall function grid points in the region downstream of the step for a distance of $6W_1$. The value of 0·03 was chosen on the basis that it represents a reasonable average over the distribution of C_μ computed by Leschziner and Rodi.[13]

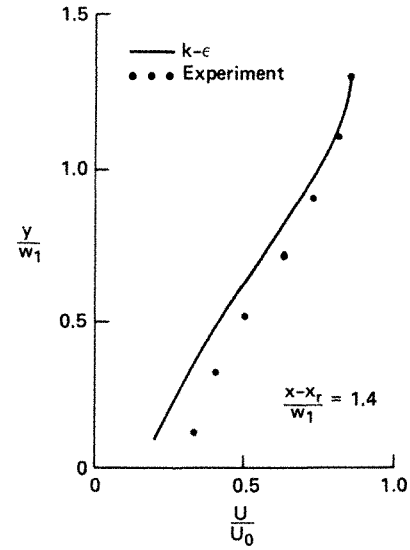

Figure 7. Comparison of standard (k–ε) model predictions with the experimental velocity measurements of Moss *et al.*[5]

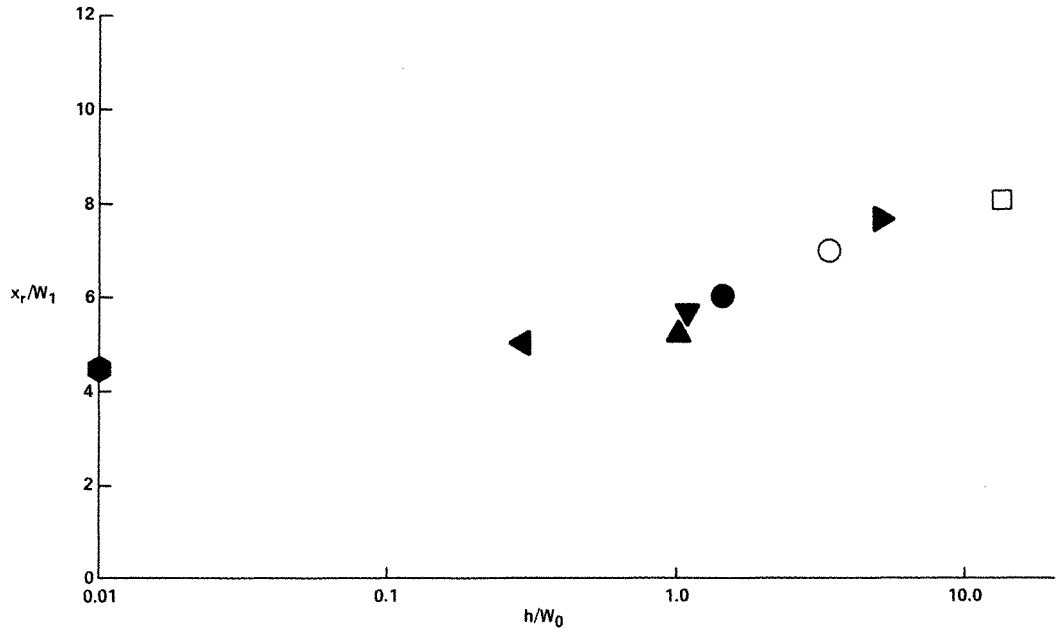

Figure 8. Plot of non-dimensional reattachment length measurements versus the inlet channel aspect ratio: ● Abbott and Kline[14]; ◆ Mohsen *et al.*[15]; ▼ Moss *et al.*[5]; ○ Kim *et al.*[16]; ◀ Etheridge and Kemp[17]; ▶ Davis and Snell[18]; □ Armaly *et al.*[19]; ▲ Durst and Tropea[12]

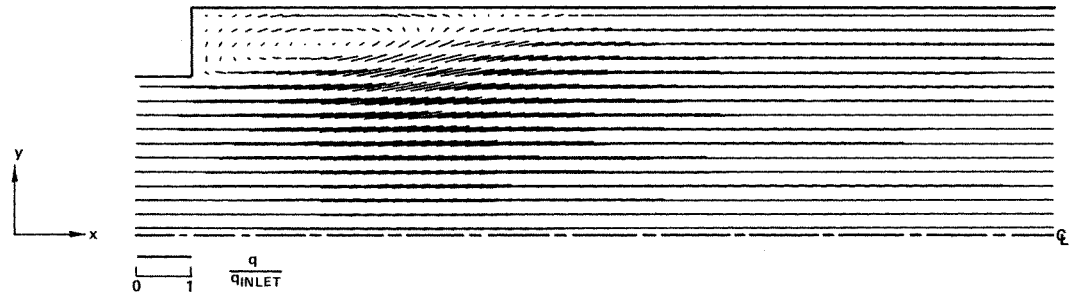

Figure 9. Depth-averaged velocity field for curvature corrected (k–ε) model simulation. Note: grid points are located at the midpoints of the velocity vectors

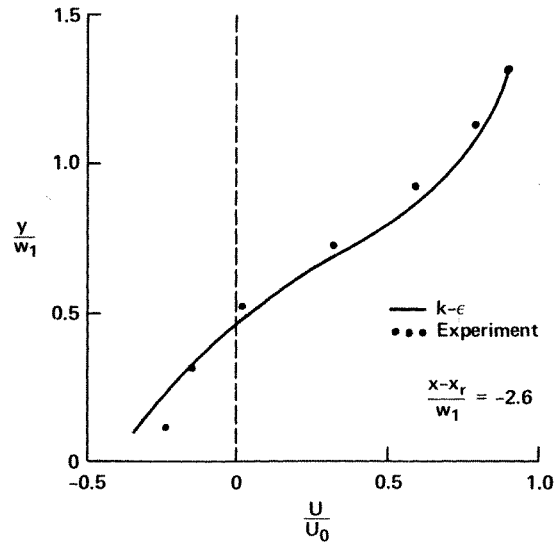

Figure 10. Comparison of curvature (k–ε) model predictions with the experimental measurements of Moss *et al.*[5]

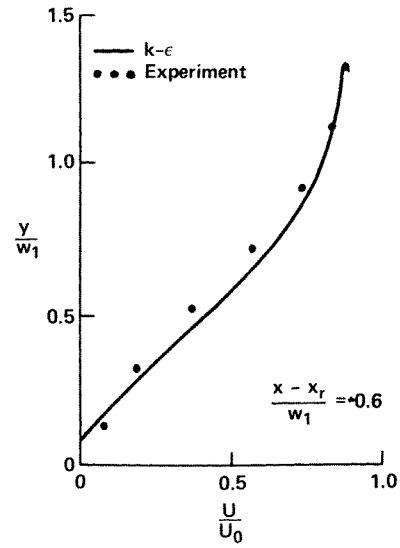

Figure 11. Comparison of curvature corrected (k–ε) model predictions with the experimental measurements of Moss *et al.*[5]

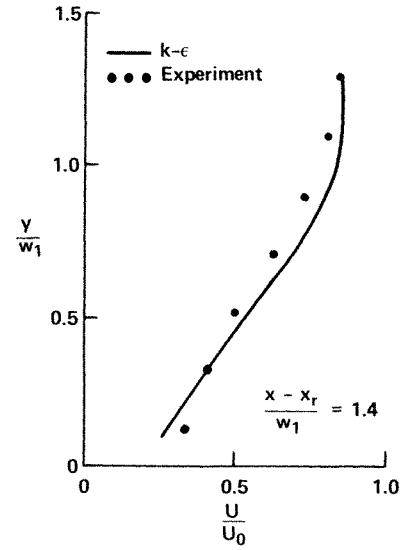

Figure 12. Comparison of curvature corrected (k–ε) model predictions with the experimental measurements of Moss *et al.*[5]

Examination of Figure 9, a vector plot of the depth-averaged velocities, reveals a significant increase in the non-dimensional reattachment length x_r/W_1, resulting from curvature modification. The predicted value in this simulation is approximately $x_r/W_1 = 4{\cdot}6$ which agrees well with the experimental measurement depicted in Figure 8. In addition, a marked improvement is seen in the comparison of the velocity profiles in the region near reattachment (Figures 10–12).

SUMMARY AND CONCLUSIONS

In summary, a test application of the depth-integrated k–ε turbulence closure model has been presented for separated flow in a wide, shallow, rectangular channel with an abrupt, symmetric expansion in width. The well-known numerical problems associated with the use of upwind and central differencing for convection have been overcome by the adaption of the spatially third-order accurate QUICK finite difference method. Based on the numerical tests performed, it can be concluded that use of the standard depth-integrated k–ε turbulence model results in a significant underprediction of the non-dimensional reattachment length (x_r/W_1). However, when the depth-integrated k–ε model was modified, by means of an *ad hoc* streamline curvature correction, a marked improvement in the model predictions resulted. Consequently, the effects of depth-mean streamline curvature have been shown to be significant, which suggests that future work is needed to examine the relationship between streamline curvature correction in the depth-integrated k–ε model and the neglected contribution of momentum dispersion.[1]

ACKNOWLEDGEMENT

This research is supported by the U.S. National Science Foundation, Grant No. CME-8004364.

REFERENCES

1. C. Flokstra, 'The closure problem for depth averaged two-dimensional flows', *Paper A106, 17th IAHR Congress*, Baden-Baden, Germany, 1977.

2. J. Kuipers and C. B. Vreugdenhil, 'Calculation of two-dimensional horizontal flow', *Report S 163-1*, Delft Hydraulics Laboratory, 1973.
3. M. B. Abbott and C. H. Rasmussen, 'On the numerical modeling of rapid expansions and contractions in models that are two-dimensional in plan', *Paper A104, 17th IAHR Congress*, Baden-Baden, Germany, 1977.
4. B. P. Leonard, 'A stable and accurate convective modelling procedure based on quadratic upstream interpolation', *Computer Methods in Applied Mechanics and Engineering*, **19,** (1979).
5. W. D. Moss, S. Baker and L. J. S. Bradbury, 'Measurements of mean velocity and Reynolds stresses in some regions of recirculating flow', *Proceedings, Symposium on Turbulent Shear Flows*, Pennsylvania State University, Vol. 1, 1977.
6. J. K. Eaton and J. P. Johnston, 'A review of research on subsonic turbulent flow reattachment', *AIAA Journal*, **19,** (9), (1981).
7. A. Rastogi and W. Rodi, 'Prediction of heat and mass transfer in open channels', *Journal of the Hydraulic Division, ASCE*, **HY3,** (1978).
8. O. J. Hinze, *Turbulence*, McGraw-Hill, New York, 1959.
9. R. S. Chapman, 'Numerical simulation of two-dimensional subcritical flow in a symmetric open channel expansion using the depth-integrated two-equation (k–ε) turbulence model', *A Doctoral Dissertation*, Virginia Polytechnic Institute and State University, 1982.
10. B. E. Lauder and D. B. Spalding, 'The numerical calculation of turbulent flows', *Computer Methods in Applied Mechanics and Engineering*, **3,** (1974).
11. F. B. Hildebrand, *Introduction to Numerical Analysis*, McGraw-Hill, New York, 1956.
12. F. Durst and C. Tropea, 'Turbulent, backward-facing step flows in two-dimensional ducts and channels', *Proceedings, Third Symposium on Turbulent Shear Flows*, University of California, Davis, September 1981.
13. M. A. Leschziner and W. Rodi, 'Calculation of annular and twin parallel jets using various discretization schemes and turbulence-model variations', *Journal of Fluids Engineering, Transactions, ASME*, **103,** (1981).
14. D. E. Abbott and S. J. Kline, 'Experimental investigation of subsonic turbulence flow over single and double backward facing steps', *Journal of Basic Engineering, Transections, ASME*, **84,** (1962).
15. A. M. Mohsen, 'Experimental investigation of the wall pressure fluctuation in subsonic separated flows', Boeing Company, *Report # D6-17094*, 1967.
16. J. Kim, S. J. Kline and J. P. Johnston, 'Investigation of separation and reattachment of a turbulent shear layer: flow over a backward-facing step', *Report MD-37*, Thermosciences Division, Department of Mechanical Engineering, Stanford University, April 1978.
17. D. W. Etheridge and P. H. Kemp, 'Measurements of turbulent flow downstream of a rearward-facing step', *Journal of Fluid Mechanics*, **86,** (3), (1978).
18. T. W. Davis and D. J. Snell, 'Turbulent flow over a two-dimensional step and its dependence upon upstream flow conditions', *Proceedings, Symposium on Turbulent Shear Flows*, Pennsylvania State University, Vol. 1, 1977.
19. B. F. Armaly, F. Durst and V. Kottke, 'Momentum, heat and mass transfer in backward-facing step flows', *Proceedings, Third Symposium on Turbulent Shear Flows*, University of California, Davis, September 1981.